Received: 11 September 2017 | Accepted: 19 October 2017

DOI: 10.1111/jace.15307

ORIGINAL ARTICLE

Journal of the American Ceramic Society

Strength of brittle materials in moderately corrosive environments

Robert F. Cook

Materials Measurement Science Division, National Institute of Standards and Technology, Gaithersburg, Maryland

Correspondence
Robert F. Cook, Materials Measurement Science Division, National Institute of Standards and Technology, Gaithersburg, Maryland.
Email: robert.cook@nist.gov

Funding information
National Institute of Standards and Technology

Abstract

The strengths of four brittle materials—cordierite glass ceramic, fused silica, silicon, and polycrystalline alumina were measured after exposure to weakly corrosive water and moderately corrosive buffered HF (BHF) solution. Exposure to water did not alter the strengths in subsequent inert strength tests and decreased the strengths in reactive strength tests. Exposure to BHF increased the strengths in both tests, but only after an incubation exposure time. Prior to the incubation time, the BHF had the same effect as water, suggesting that the bond rupture kinetics were unaffected. Examination of strength-controlling indentation flaws after the incubation time showed clear corrosive effects on the flaw geometry indicative of reductions in the indentation residual stress fields. The implication is that moderately corrosive environments increase the strength or lifetime of a brittle component by reducing the crack driving force via flaw alteration and do not, as perhaps expected, decrease the strength or lifetime through enhanced chemical reactivity.

KEYWORDS

brittle materials, corrosion/corrosion resistance, cracks/cracking, indentation, strength

1 | INTRODUCTION

Ceramic materials have great potential for use in corrosive environments—as structural components that resist environmental attack (e.g., mechanical seals in oil recovery systems[1]) or as coatings that protect underlying structural components (e.g., veneers on dental restorations[2]). Prediction of the mechanical reliability of ceramics on exposure to such environments is critical to their successful application. However, the phenomena on which such predictions are based are conflicting, rendering prediction difficult and thus reliable application uncertain. A quantitative measure of reliability is the maximum sustainable load that a component can support, or, alternatively, the strength that a material exhibits on exposure to a corrosive environment. In particular, strengths have been observed to increase on exposure to water[2,3] or, more in accord with expectation, decrease,[1,4,5] a divergence in behavior that has been known for some time[3,4] and extends to the present.[1,2,5]

The mechanical reliability of brittle materials such as ceramics, glasses, and semiconductors is usually decreased in a corrosive environment. A typical example is shown in Figure 1, which shows the decrease in strength of a cordierite glass ceramic on exposure to water.[5] The glass-ceramic samples all contained the same dominant controlled flaw—a Vickers indentation formed with an indentation load of P = 20 N. The hatched band to the left of the figure represents the "inert" strength, σ_{max}, of the samples in the absence of corrosive species. This is the maximum strength that the indented samples can exhibit. The open symbols represent the "reactive" failure strengths, σ_f, of the samples in water at the applied stressing rates, $\dot{\sigma}_a$, indicated (top axis). For all the $\dot{\sigma}_a$ values shown in Figure 1, the reactive strengths are less than the inert strength, $\sigma_f < \sigma_{max}$, demonstrating the effect of water on the

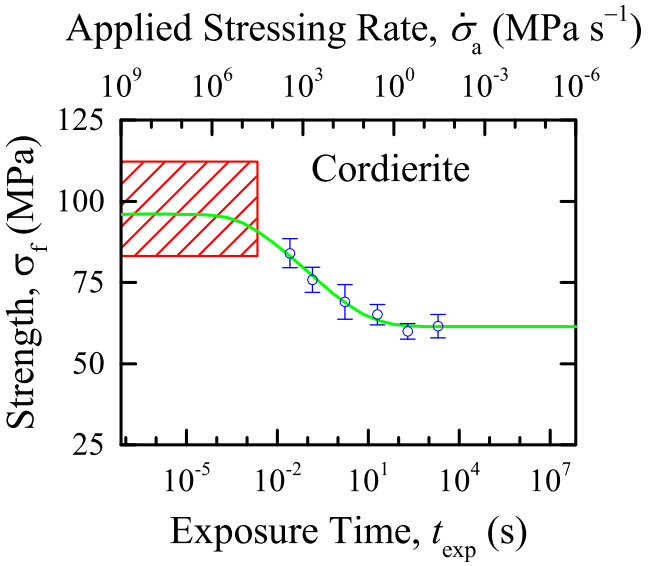

FIGURE 1 Strength of cordierite glass ceramic as a function of applied stressing rate (top)[5] or failure time (bottom) for measurements in water. Samples contained 20-N Vickers indentation flaws. Inert strength shown at left [Color figure can be viewed at wileyonlinelibrary.com]

enhanced propagation of the strength-controlling indentation cracks. At small $\dot{\sigma}_a$ (right of figure) the reactive strengths approach an invariant plateau value, σ_{min}, that is the minimum strength that the indented samples can exhibit. The solid line in Figure 1 represents the best fit of a nano-scale stress-corrosion cracking (SCC) model[5] to σ_f that includes σ_{max} and σ_{min} as the visible upper and lower strength asymptotes. The atomic-scale kinetics of the SCC water reaction with the material determines the $\dot{\sigma}_a$-dependent transition between the two strength bounds: the solid line in Figure 1 and elsewhere[5] are examples in which the corrosive phenomenon is well characterized and hence reliability predictions can be made.

However, another way of representing the data of Figure 1 is to recognize that the time, t_{exp}, given by $t_{exp} = \sigma_f / \dot{\sigma}_a$, is the time that a sample was exposed to corrosive environment and this is also shown in Figure 1 (bottom axis). (Here, the exposure time was one during which the applied stress was increasing and hence in this case the exposure time was also the failure time.) The chemical exposure and mechanical measurement were thus occurring simultaneously. It is possible to isolate the chemical effects from the mechanical response by arranging for the exposure and measurement to occur *sequentially*, as shown in Figure 2.[6,7] In Figure 2A, an indentation-inert strength sequence is shown. In step A(1), a sample is indented, forming a residual indentation deformation zone and half-penny cracks. In step A(2), the sample is broken, usually in bending, in an inert environment, usually in 50 ms or less, measuring the stress to unstably propagate the indentation cracks, the inert strength. In Figure 2B, an

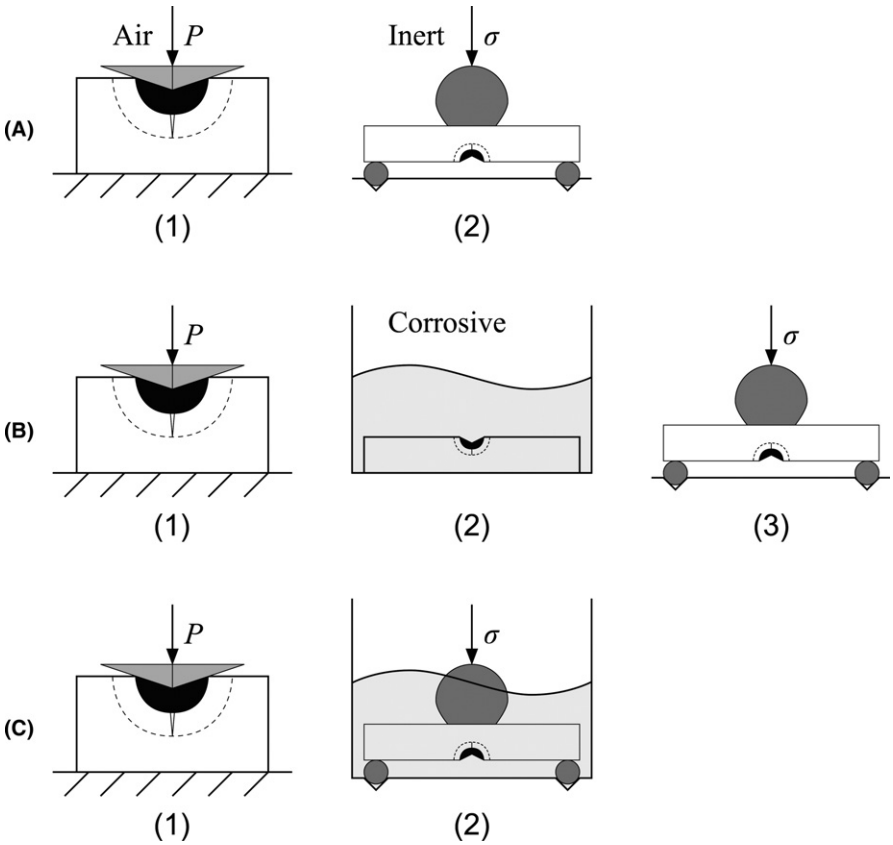

FIGURE 2 Schematic diagrams (not to scale) of indentation-strength measurement sequences. (A) Indentation (1) followed by inert strength measurement (2). (B) Indentation (1) flowed by aging in a corrosive environment (2) followed by inert strength measurement (3). (C) Indentation (1) followed by reactive strength measurement in a corrosive environment (2)

indentation-corrosive exposure-inert strength sequence is shown. In step B(1), a sample is indented as before. In step B(2), the indented sample is exposed to a corrosive environment for various periods of time (aged) from seconds to hours under zero applied stress. In step B(3), the sample is broken in an inert environment as before. In Figure 2C, an indentation-reactive strength sequence is shown. In step C (1), a sample is indented as before. In step C(2), the indented sample is exposed to a corrosive environment under increasing applied stress until the sample breaks and the reactive strength is measured. Figure 2A corresponds to the hatched band in Figure 1; Figure 2C corresponds to the open symbols in Figure 1. Here, sequence 2A will be referred to as an inert strength test, sequence 2B will be referred to as zero-stress aged strength test, and sequence 2C will be referred to as a reactive strength test.

The sequences in Figure 2B and C are the focus of the work here. It can be argued that the success of the nano-scale model used to describe the data in Figure 1 depends on the constancy of the meso-scale indentation parameters during the reactive strength test. *Before* an inert or reactive strength test the parameters may depend on indentation load[8] and may relax after indentation,[9] especially if the indentations are annealed,[10] or deliberately thermally altered[11,12] but the parameters are then invariant *during* the test.[5] It can also be argued that such invariance (and hence the success of the model) is a consequence of the weakly corroding effect of water—a well-known SCC environment for oxide materials.[13] Hence, to exacerbate the effects of corrosion on the strength of brittle materials, a moderately corrosive environment, an aqueous HF solution, was used here in the chemical exposure steps B(2) and C(2). A similar HF solution was used previously on soda-lime silicate glass (SLG) for a similar purpose,[6,9,14] (in buffered or modified form) on silicon,[6,15,16] and also (in vapor form) on tungsten carbide-cobalt.[17] The words strong, moderate, and weak are used here in a particular way: A strongly corrosive environment is one that *removes* (say, by dissolution) material from a flat, flaw-free surface.[9,14,18] The effects of such an environment were important in developing the early rate-based models of SCC in ceramics.[19-21] A moderately corrosive environment is one that attacks surface flaws leaving the surrounding material largely intact.[1] Such an environment is the predominant focus of the work here. A weakly corrosive environment *reacts* with freshly broken or strained bonds in a material, but otherwise does not remove material from surfaces or flaws. Such a reactive environment was envisaged in early considerations of fracture[22] and was important in developing the more recent force-based models of SCC in ceramics.[23,24]

The following section describes the materials and procedures used, building on the schematic diagrams of Figure 2. This is followed by the experimental results, classifying the effects of environments on materials by the strongly, moderately, and weakly corroding definitions given above. The results consist of both strength variation measurements and indentation observations. The major goals of the work are to provide a qualitative survey of the effects of corrosive environments on strength, thereby placing the previous nano-scale models[5,23,24] in context and placing limitations on the application of such models to *strength* prediction in corrosive environments. The Discussion points to how the data might be interpreted or used in a quantitative reliability sense.

2 | EXPERIMENTAL PROCEDURE

2.1 | Materials and indentation

Four brittle materials, covering the range of corrosive influences, were studied for the effects of exposure to a corrosive environment on strength. The materials were a cordierite ($2MgO{\cdot}2Al_2O_3{\cdot}5SiO_2$) glass ceramic as shown in Figure 1 and studied elsewhere,[5,25] fused silica (amorphous SiO_2), a doped p-type silicon (Si),[7] and glass-bonded polycrystalline alumina (Al_2O_3) (Coors AD96, Coors Ceramic Company, Golden, CO). The cordierite glass ceramic samples were identical to the base (B) material in a previous work,[25] and were in the form of discs 35 mm in diameter × 3 mm thick. The cordierite was almost completely crystalline with crystallite size 3-15 μm. The SiO_2 samples were in the form of laser window discs 25 mm diameter × 1 mm thick. The Si samples were single crystal (001) discs 35 mm diameter × 3 mm thick. The Al_2O_3 samples were in the form of squares with 36 mm × 36 mm sides × 2 mm thick. The average Al_2O_3 crystallite size was 6 μm and the volume fraction of crystallites was 89%. The cordierite, fused silica, and silicon sample surfaces were received polished. The alumina sample surfaces were received as sintered; a few samples were polished for microscopy. All sample surfaces were untreated prior to testing.

Prior to strength testing, all samples were indented in air with a four-sided Vickers diamond pyramid in the center of a prospective test face. The indentation load for the cordierite, fused silica, and alumina samples was P = 10 N; that for the silicon samples was P = 2 N with indentation diagonals aligned along <110>. A schematic top-view diagram of a Vickers indentation flaw is shown in Figure 3A, indicating the square residual contact impression dimension a and the half-penny crack surface trace length c. A schematic side-view diagram of the flaw is given in Figure 3B, showing the subsurface plastic deformation zone localized beneath the contact impression and the half-penny cracks. The strain mismatch between the localized plastic deformation zone and the surrounding

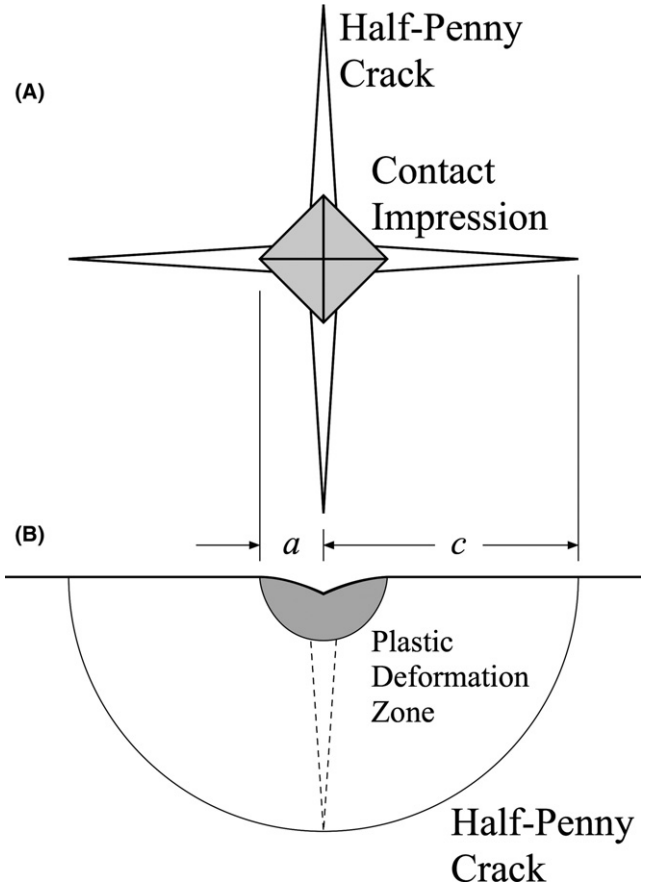

FIGURE 3 Schematic diagrams of an ideal Vickers indentation flaw showing half-penny crack and contact impression dimensions: (A) Surface plan view and (B) Cross-section view

elastic matrix gives rise to a residual stress field in the matrix that is responsible for initiating and stabilizing the half-penny cracks. The half-penny cracks form perpendicular to the material surface and it is these that propagate under an applied stress to cause component failure. At large indentation loads another set of cracks form, the lateral cracks, which initiate and stabilize parallel to the material surface. Lateral cracks release the constraint of the matrix on the plastic deformation zone, thereby reducing the indentation residual stress field and increasing the applied stress required for component failure. The indentation loads used here were selected to be small such that the indentation patterns in the materials were as "ideal" as possible (as per Figure 3) with maximum residual stress, yet large enough to be the dominant flaw in a component and responsible for component failure. No lateral cracks were visible at the indentations on the material surfaces prior to strength testing.

2.2 | Corrosive exposure and strength testing

The samples were mounted in flat-on-three-ball biaxial flexure rigs for strength testing, with the indentation flaw centered on the tensile face. The radii of the inner, upper flats were 1.5 mm for the fused silica samples, 2 mm for the cordierite and silicon samples, and 2.5 mm for the alumina samples. The radii of the outer, lower circles, on which the samples were supported by the three balls were 10 mm for the fused silica samples and 16 mm for the cordierite, silicon, and alumina samples. Failure stresses, σ, were calculated from failure loads, F, by $\sigma = kF/d^2$, where d is the sample thickness and k is a geometry term that depends on rig and sample dimensions;[26,27] for the rig dimensions here, k was about 1.5. Failure loads were measured by resistance load cell for tests lasting longer than about 10 second and by piezoelectric load cell for tests lasting less than about 10 second.

Three types of strength tests were performed.[7] In the first, an inert strength test (Figure 2A), the indented samples were loaded to failure in 50 ms or less. The indentation flaws were covered with a drop of silicone oil prior to testing. Both the rapid failure time and the oil drop impeded the diffusion of ambient water vapor to the indentation cracks during failure and led to inert conditions. At least six measurements were performed for each material, to arrive at an estimate of σ_{max}, the maximum strength for the indented components. In the second type of test, a zero-stress aged strength test, inert strength was measured following an exposure to a corrosive environment (Figure 2B). Following indentation, the samples were immersed in either distilled water (H_2O, pH = 7) or an aqueous, NH_4-buffered 0.1 mol·L^{-1} HF solution (BHF, pH = 4.5) under zero stress in simple containers for exposure times, t_{exp}, of 1 second to 24 hour. The samples were then rinsed in water and hot-air-dried. An inert strength test was then performed as above. In the third type of test, a reactive strength test, strength was measured in a corrosive environment (Figure 2C). Following indentation, the samples were placed in the flexure rig immersed in either H_2O or BHF. The samples were then loaded to failure by a linearly increasing force, varying the applied stressing rate, $\dot{\sigma}_a$, over at least six decades, such that the conjugate exposure time, varied similarly, from about 50 ms to more than several hours. In some cases, the samples were not broken, but observed in the scanning electron microscope (SEM). The combination of the schemes in Figure 2A and C is a well-established methodology for strength testing and reliability prediction in a weakly corrosive environment.[5] The intent here is to demonstrate a methodology for strength testing in a moderately corrosive environment as in Figure 2B and C.

3 | RESULTS

Figure 4 shows the variation of strength with exposure time, t_{exp}, for P = 10 N indented cordierite glass-ceramic

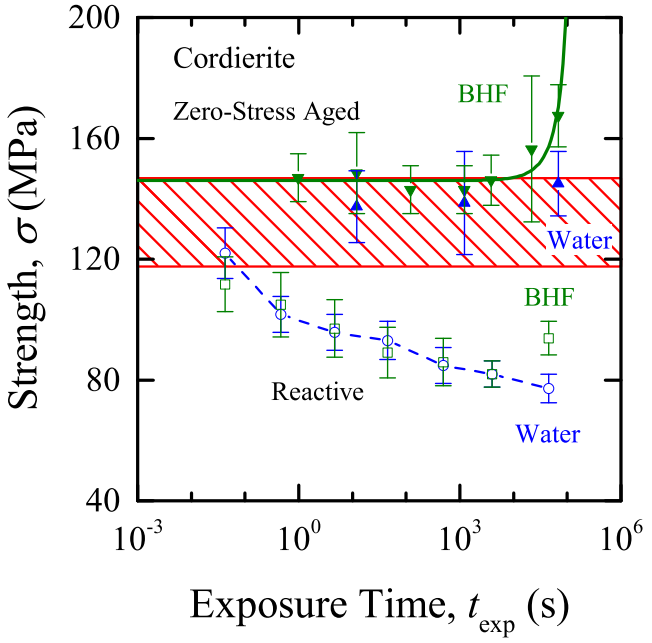

FIGURE 4 Strength of cordierite glass ceramic as a function of exposure time to water or buffered HF (BHF) solution. Samples contained 10-N Vickers indentation flaws. Inert strength shown as the hatched band; zero-stress aged inert tests shown as solid symbols; reactive tests shown as open symbols. Bars indicate standard deviations [Color figure can be viewed at wileyonlinelibrary.com]

samples. The hatched band represents the inert strength, σ_{max}, the solid and open symbols represent zero-stress aged and reactive strengths, respectively, at the exposure times indicated; σ is taken to represent a strength generally. In all cases (and unless otherwise indicated, throughout the paper) the band and symbols represent the means and standard deviation limits of at least five experimental measurements. The hatched band and the open circular symbols are directly analogous to those in Figure 1, representing inert tests and tests in water, respectively; the dashed line joins the means of the open circular symbols as a guide to the eye. The solid line is discussed below.

The reactive strengths in water (open circular symbols, measured with increasing stress as in Figure 2C) display the same behavior as well-described by the nano-scale model in Figure 1: There is a rapid initial effect (less than 1 s exposure was required to decrease strength) followed by a decreasing, but convex variation in strength with exposure time. The reactive strengths in BHF (open square symbols, measured as in Figure 2C) display a similarly initial rapid effect but eventually a much greater convexity such that at long exposure times the reactive strength actually displays an *increase*. The solid symbols represent inert strengths following zero-stress aging in a corrosive environment (measured as in Figure 2B) at the exposure times indicated. For both water and BHF environments, the strengths at short exposure times were not degraded and were in fact at the upper edge of the inert strengths (in earlier studies in SLG the aged strengths exceeded the inert strength[3,6,28]). At the longest exposure time, nearly 10^5 second (about a day), the samples exposed to water continued this behavior (similar invariance was observed in alumina containing indentation or scratch flaws[27]). The samples exposed to BHF, however, were significantly greater in strength and exceeded the inert strengths at the longer exposure times (also observed in SLG[2]). Clearly, the zero-stress aging in a corrosive environment caused the strength-controlling indentation flaws to become less potent prior to the inert strength test. This effect was particularly pronounced on BHF exposure and probably also caused the observed increased strength at the longest exposure times in the reactive strength tests.

Figure 5 shows SEM images of the effects of zero-stress aging in BHF on 10 N indentation flaws in cordierite glass-ceramic. Figure 5A shows an as-indented, un-aged sample. Figure 5B shows a sample aged for 18 hour in BHF. Figure 5A appears much as the schematic plan view of the ideal indentation in Figure 2A, particularly the sharp edges of the residual contact impression and the clearly visible surface traces of half-penny cracks. The contact impression in Figure 5B is not well formed, is much shallower than the un-aged impression in Figure 5A, and appears to be partially removed from the surrounding material by the formation of peripheral cracks (right) and dissolved material (left). Cracks are visible on the material surface, but their meandering paths suggest that they are not the traces of half-penny cracks but part of a surface fragmentation pattern originating at the contact impression. The overall view is of a surface that has had material partially removed by dissolution, particularly at the indentation flaw (as in SLG[6]), which is breaking up. Both the removal of the surface (reducing the half-penny crack size[14]) and the removal of the indentation plastic deformation zone (reducing the residual field) lead to a reduction in flaw potency and thus an increase in strength, consistent with Figure 4. Figure 6A shows a schematic cross-section of the effects of the BHF zero-stress aging on the cordierite glass-ceramic. The images of Figures 5B and 6A represent a moderately to strongly corrosive effect.

To place the fused silica strength measurements to follow in context, Figure 7 shows SEM images of three P = 10 N indentations in fused silica formed under nominally identical conditions. The indentation flaws exhibit a diversity of behavior, including deviations from ideality such as ring cracking, lateral cracking, cone cracking, and "punching in" of the contact impression.[29] The deviations increase in the order A, B, C: cone cracking, and punching in are particularly evident in Figure 7C. These deviations reflect a reduction in the residual stress, and, when they occur, lead to an increase in strength. As a consequence,

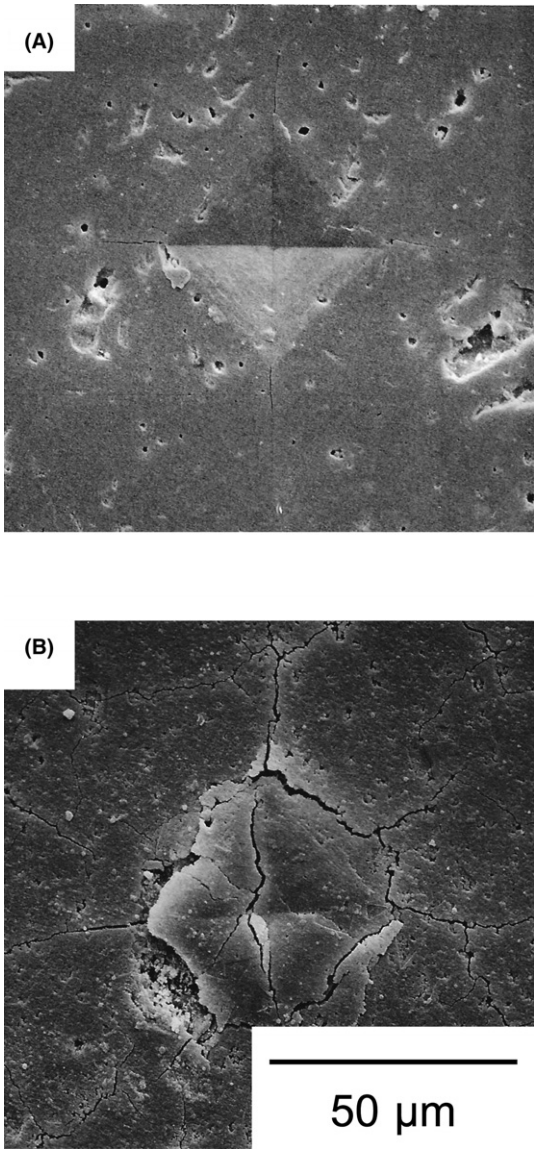

FIGURE 5 Scanning electron micrographs of 10-N Vickers indentation flaws in cordierite glass ceramic. (A) As-indented; (B) Exposed to buffered HF solution for 18 hour

"natural" indentation strength distributions in fused silica include a number of high strengths reflecting the occurrence of residual-stress reduced flaws as in Figure 7C. The skewed strength distribution (large outlier strengths) needs to be considered in aging studies.

Figure 8 shows the variation in strength, σ, with exposure time, t_{exp}, for P = 10 N indented fused silica samples. The hatched band and closed and open symbols represent the inert strength, aged strengths, and reactive strengths as in Figure 4. Distinct from Figure 4, the widths of the band and the bars represent the *ranges* of the measurements, taking into account the variability evident in Figure 7. The asymmetry of some of the bars, particularly at long exposure times, reflects the significant reduction in residual field and hence the increase in strength of some samples. (Symmetric standard deviation bars would not reflect the outliers; the bars here do not represent the same statistical information as standard deviations.) The variations of the strengths of fused silica in reactive environments are almost identical to those of cordierite glass ceramic (Figure 5): Rapid and convex variation of reactive strength with exposure time, with greater convexity and strength increase at long exposure times for samples in BHF. After a delay, zero-stress aged samples exposed to BHF greatly exceeded the inert strengths at the longer exposure times; water had little aging effect. Once again, zero-stress aging in a corrosive environment caused the indentation flaws to become less potent and was associated with an observed increased strength at the longest exposure times in the reactive strength tests.

Figure 9 shows SEM images of the effects of zero-stress aging in BHF on a 10 N indentation flaw in fused silica. Figure 9A shows the as-indented, near-ideal, unaged sample from Figure 7A. Figure 9B and C show samples aged for 1 hour and 18 hour, respectively, in BHF. The two most striking features of Figure 9B and C in comparison with Figure 9A are the disappearance of the contact impression and the appearance of a dominant cone crack much larger in size than the initial indentation. Both of these effects significantly reduce the residual field and increase the strength: etching a near-ideal indentation has similar effects to natural indentation non-ideality, compare Figures 7B and 9B and Figures 7C and 9C. It is also clear that the indentation flaw geometry has changed significantly to remove sharp cracks. It is unclear whether the corrosive environment is simply enlarging the width of a pre-existing large cone crack or extending the length and width of a small cone crack but the effect remains the same, to increase strength. (These observations are the same as those on SLG, with cone cracks replacing half-penny cracks.[6]) Figure 6B shows a schematic cross-section of the effects of the BHF zero-stress aging on fused silica. The images of Figures 6B and 9C represent a moderately corrosive effect.

Figure 10 shows the variation in strength, σ, with exposure time, t_{exp}, for P = 2 N indented Si samples.[7] The hatched band and open symbols represent the inert strength and reactive strengths as in Figure 5; the closed symbols represent individual aged strength tests. The reactive strengths in water exhibit a rapid, but small, decrease relative to the inert strength. The reactive strengths are then invariant with exposure time. The reactive strengths in BHF exhibit an increase in strength with exposure time, such that the reactive strength at the longest exposure time is greater than the inert strength. Zero-stress aging seems to have the same weak effects as reactive strength testing: slight decrease in water, slight increase in BHF. Doping has no effect.[7]

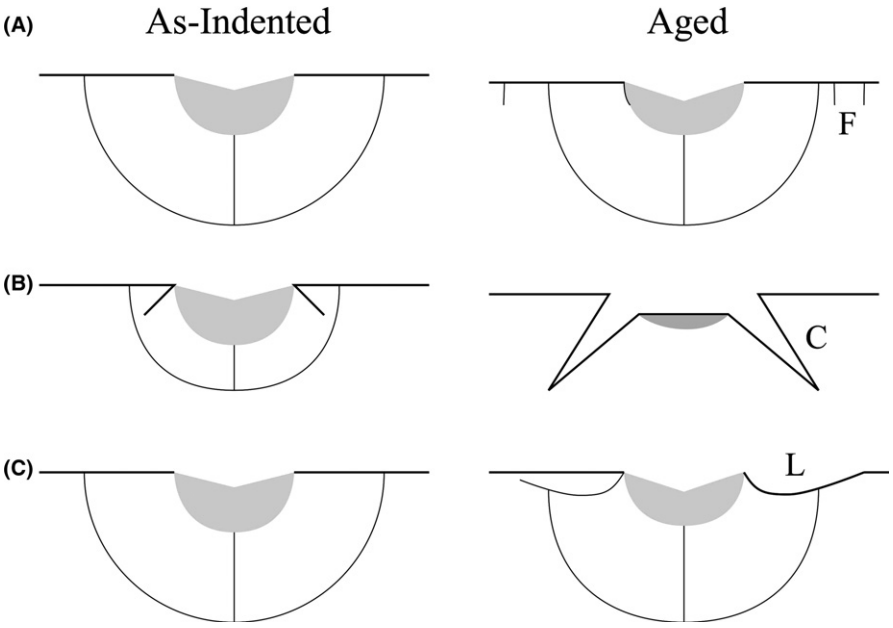

FIGURE 6 Schematic cross-sectional diagrams of corrosive aging effects on indentation flaws: Left diagrams, as-indented; right diagrams, aged. (A) Dissolution and retraction of the surface and contact impression and the formation of fragmentation cracks (labeled "F") (e.g., cordierite glass ceramic). (B), Dissolution and retraction of the surface and contact impression and the growth of cone cracks (labeled "C") (e.g., fused silica). (C) Formation and growth of lateral cracks (labeled "L") (e.g., silicon)

Figure 11 shows SEM images of the effects of zero-stress aging in BHF on a 2 N indentation flaw in Si. Figure 11A shows an as-indented, un-aged sample. Figure 11B and C show samples aged for 2 hour and 18 hour, respectively, in BHF. The un-aged sample appears ideal (Figure 3A). As in previous observations,[7,16,17] the dominant features on aging are the appearance of lateral crack chips (predominantly upper left) and the dissolution of the contact impression (primarily along the shear faults). Both of these features decrease the residual field, leading to a closing of the surface traces of the half-penny cracks (barely visible in Figure 11B and C) and are consistent with an increase in strength at long exposure times. The growth of lateral cracks in a reactive environment was recognized in earlier works as responsible for aged strength increases in SLG.[6,28] Figure 6C shows a schematic cross-section of the effects of the BHF zero-stress aging on Si. The images of Figures 6C and 11C represent a weakly corrosive effect.

Figure 12 shows the variation in strength, σ, with exposure time, t_{exp}, for P = 10 N indented Al_2O_3 samples. The hatched band and closed and open symbols represent the inert strength, aged strengths in water, and reactive strengths in water as in Figure 5. The variations of the strengths of Al_2O_3 in water are almost identical to those of cordierite glass ceramic (Figure 5) and fused silica (Figure 8): Rapid and convex variation of reactive strength with exposure time, and small increasing effect of exposure time on the strengths of zero-stress aged samples relative to the inert strength (somewhat contrary to invariant effects previously observed in alumina[27]). SEM images of indentations in Al_2O_3 aged in water showed no visible effects. The measurements in Figure 12 and the SEM observations typify a weakly corrosive effect.

4 | DISCUSSION AND CONCLUSIONS

Perhaps the most surprising result of this new, detailed study—involving four materials, three testing protocols, and three environments—is that moderately corrosive environments can *increase* the strengths of brittle materials. This result is opposed to that in weakly corrosive, or merely reactive, environments in which the environment is leads to a strength decrease.[1] These results, although extremely important for brittle material reliability predictions, reflect strength measurements under different circumstances and so it is useful to be clear about the phenomenology observed, here and elsewhere:

1. Exposure to a weakly corroding or reactive environment, zero-stress aging in H_2O, prior to an inert strength test (Figure 2B) did not have a significant effect on the inert strength (Figures 4, 8, 10, 12) of any material. The small strength increases probably reflected saturating lateral crack growth and related residual field decreases, observed previously.[5,6,9,10,17,28] The strength increases measured in abraded samples[3] probably also reflected less-easily observed residual field decreases.
2. Exposure to a weakly corroding environment during an increasing stress test in H_2O (Figure 2C) led to a significant decrease in reactive strength (Figures 4, 8, 10, 12). The strengths of all four materials studied would be well described by the "standard model" of kinetics+reactive equilibrium for crack growth and strength.[5,24]
3. Exposure to a moderately corroding environment, zero-stress aging in BHF, prior to an inert strength test (Figure 2B) led to a significant increase in the inert strength (Figures 4, 8, 10) of three materials, similar to that

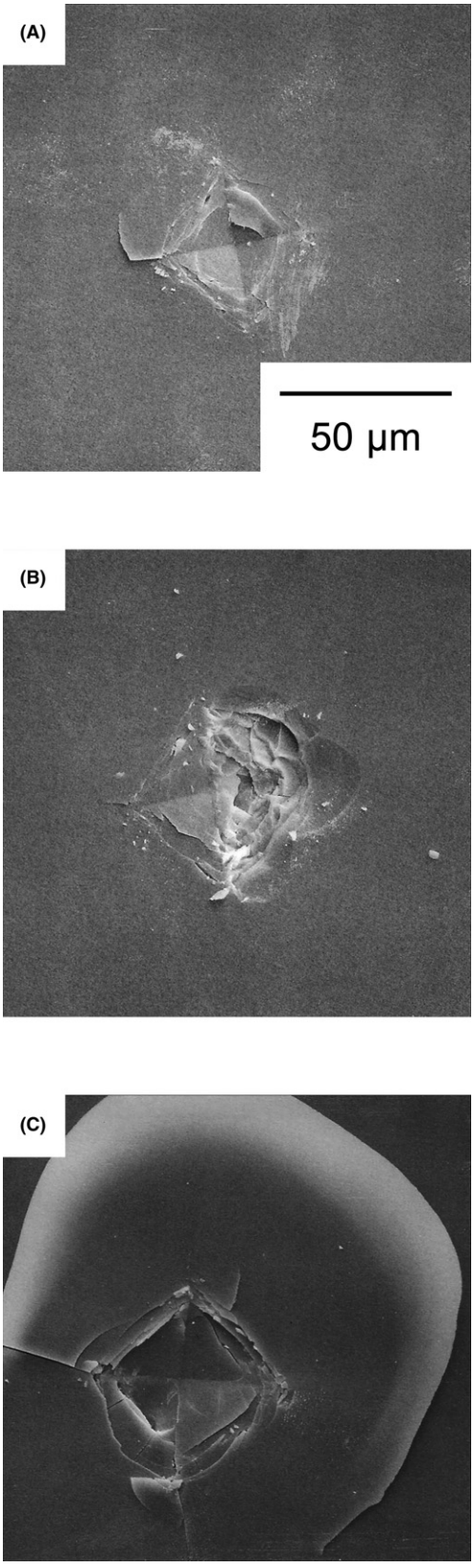

FIGURE 7 Scanning electron micrographs of 10-N Vickers indentation flaws in fused silica showing the diversity of non-ideal disrupted indentation responses, including suppressed half-penny crack formation and cone crack formation. (A) Near ideal. (B) Partially disrupted. (C) Completely disrupted

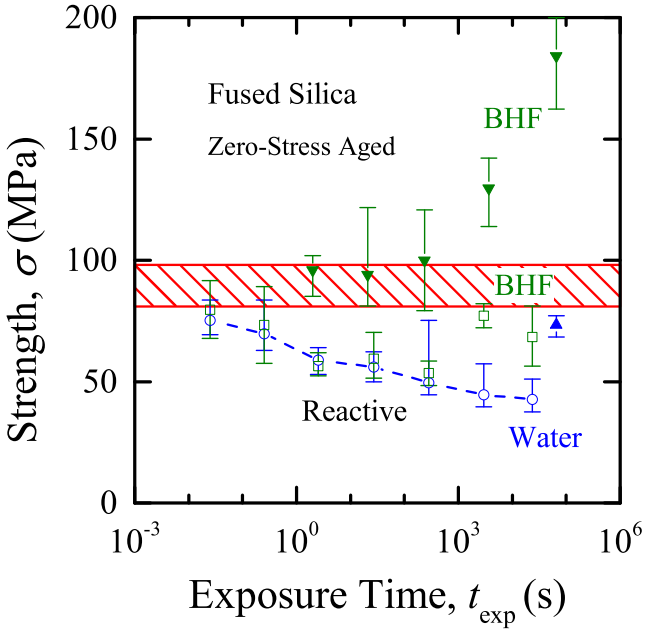

FIGURE 8 Strength of fused silica as a function of exposure time to water or buffered HF (BHF) solution. Samples contained 10-N Vickers indentation flaws. Symbols as in Figure 4, except bars indicate ranges [Color figure can be viewed at wileyonlinelibrary.com]

observed in earlier studies,[6,14] but only after an "incubation" exposure time. Prior to the incubation time, the inert strengths were largely unaffected.

4. Exposure to a moderately corroding environment during an increasing stress test in BHF (Figure 2C) led to a significant decrease in reactive strength (Figures 4, 8, 10) nearly identical to the decrease observed in water, but only prior to the incubation time observed in the zero-stress aging tests. After the incubation time, the reactive strengths increased, similar to the zero-stress aged strengths.
5. Exposure to a moderately corroding environment during zero-stress aging in BHF (Figure 2C) led to significant alterations of the strength-controlling indentation flaws (Figures 5, 9, 11), including reduction in the size and opening of half-penny cracks, increase in the size of lateral and cone cracks, reduction in the size of the contact impression, and indentation-localized surface damage. Not all materials exhibited all alterations (Figure 6), with strong material dependence. (Without using controlled flaws, it is difficult to correlate the diversity of observed strength phenomena[1-4,14] with one or the other of material or flaw alteration on aging.)

Hence, the expectation that a "more corrosive" or "more reactive" environment would lead to a greater strength decrease is not borne out, although there are clear corrosive

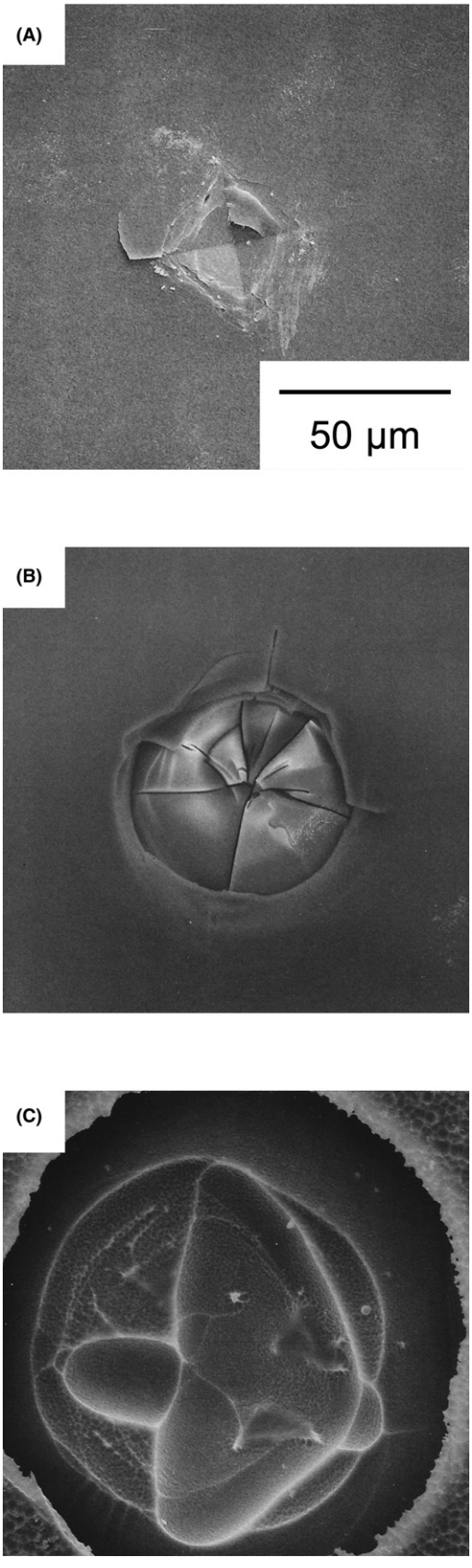

FIGURE 9 Scanning electron micrographs of 10-N Vickers indentation flaws in fused silica. (A) As-indented; (B) Exposed to buffered HF solution for 1 hour. (C) Exposed to buffered HF solution for 18 hour

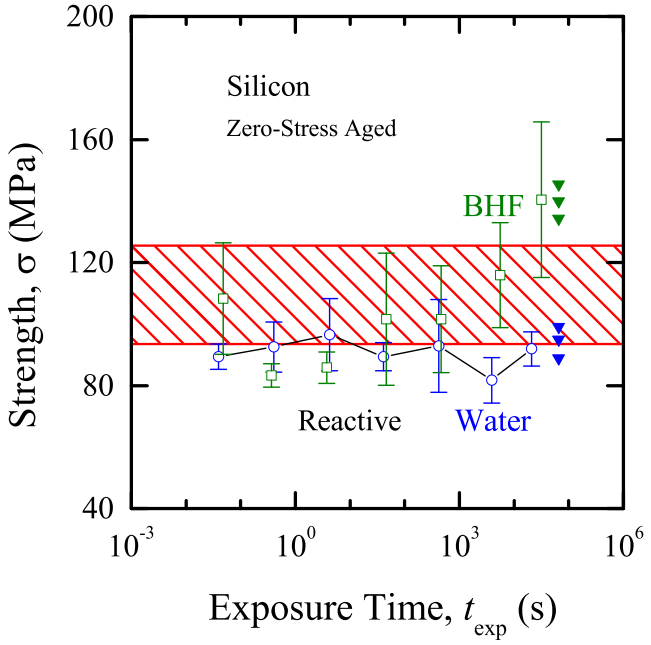

FIGURE 10 Strength of silicon as a function of exposure time to water or buffered HF (BHF) solution.[7] Samples contained 2-N Vickers indentation flaws. Symbols as in Figure 4 [Color figure can be viewed at wileyonlinelibrary.com]

effects in both inert and reactive strengths and at contact flaws. The effects can be understood in terms of exposure-time dependent parameters in the strength model developed previously for contact flaws.[5] (The effects should be seen in the context of exposure-time dependent strength *degradation* by corrosion-induced surface roughening[30,31] or debris formation[18] on initially "flaw-free" near-pristine surfaces.)

The driving force on an indentation crack (see Figure 3) formed by load P under a uniform applied stress, σ_a, in terms of the mechanical energy release rate G, is given by:

$$G = (\psi\sigma_a c^{1/2} + \chi P/c^{3/2})^2/E, \quad (1)$$

where ψ and χ are dimensionless geometry terms setting the amplitudes of the effects of applied and residual stresses, respectively, and E is the Young's modulus of the material. Setting the inert equilibrium condition, $G = 2\gamma_0$, where γ_0 is the fracture resistance ("surface energy") in an inert environment and absence of reactive species, enables the inert strength, σ_{max}, to be calculated as[21]:

$$\sigma_{max} = 3(2\gamma_0 E)^{2/3}/4^{4/3}\psi\chi^{1/3}P^{1/3}. \quad (2)$$

Observation (1) above implies that zero-stress aging in H_2O does not alter ψ or χ (the flaw geometry or residual stress) in Equation (1), thus leaving the inert strength in Equation (2) unaltered (provided the half-penny cracks do not extend by more than ~2.5 after indentation,[8,9] the

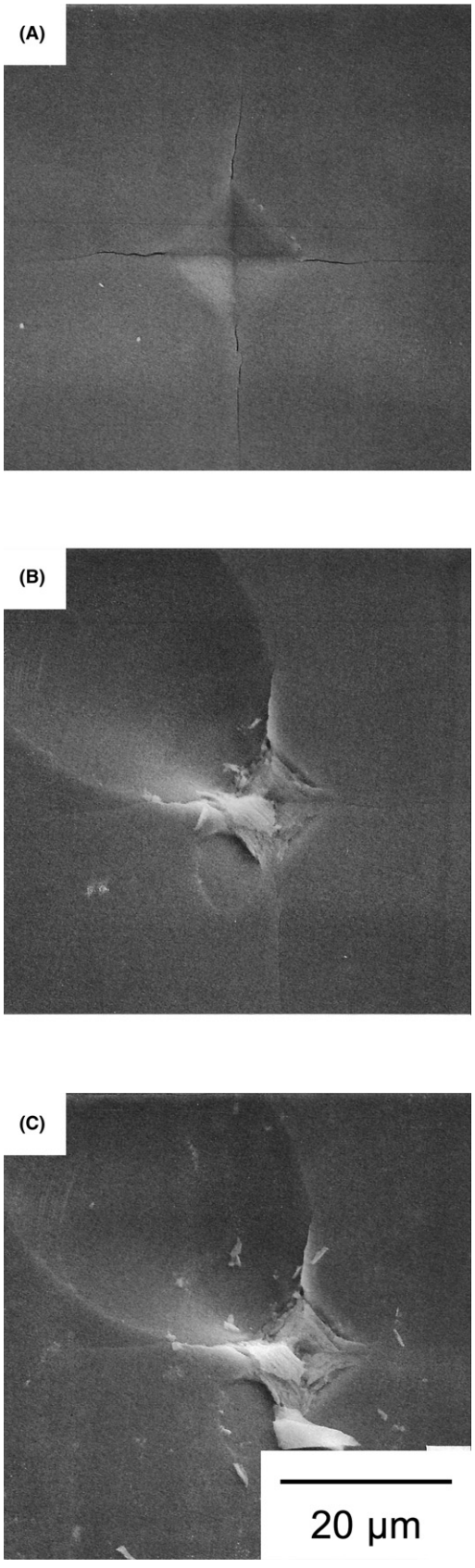

FIGURE 11 Scanning electron micrographs of 2-N Vickers indentation flaws in silicon. (A) As-indented. (B) Exposed to buffered HF solution for 2 hour. (C) Exposed to buffered HF solution for 18 hour

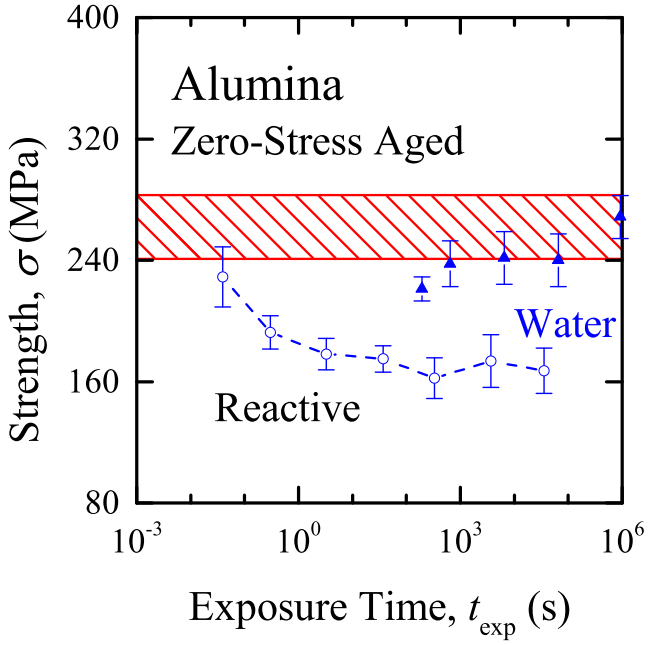

FIGURE 12 Strength of alumina as a function of exposure time to water. Samples contained 10-N Vickers indentation flaws. Symbols as in Figure 4 [Color figure can be viewed at wileyonlinelibrary.com]

residual field renders σ_{max} immune to changes in the initial crack length, as shown in Equation (2)). Observations (3) and (5) above are consistent with zero-stress aging in BHF decreasing ψ or χ in Equation (1), leading to an increase in the inert strength following Equation (2), after an incubation time. The strength model[5] can be modified analytically to account for these effects: Simple expressions including an incubation time that accomplish this are:

$$\psi = (\psi_0/A)[A - (t/t_{inc})^B] \tag{3a}$$

or

$$\chi = (\chi_0/A)[A - (t/t_{inc})^B], \tag{3b}$$

where ψ_0 or χ_0 are the initial amplitude terms at time $t = 0$, t_{inc} is the incubation time, and A and B are numerical terms. Previous observations on SLG[6] suggested that the incubation time was related to the time required for lateral crack growth (Figure 6C), in which case Equation (3b) would apply. An example is shown by the solid line in Figure 4, which combines Equations (2) and (3b) to describe the exposure time variation of the BHF-aged strength of cordierite (using $A = B = 1.5$ and $t_{inc} = 10^5$ second); the similarity with the empirical strengthening curve shown for SLG[14] is noted.

The reactive equilibrium condition is $G = 2\gamma$, where γ is the fracture resistance in a reactive environment and after saturation of reactive species. Setting this condition enables the reactive minimum strength, σ_{min}, to be calculated as[5]:

$$\sigma_{min} = 3(2\gamma E)^{2/3}/4^{4/3}\psi\chi^{1/2}P^{1/3}. \quad (4)$$

σ_{min} values appear as the lower reactive strength bounds on the right of Figures 1, 4, 10, and 12. Of equal importance in a reactive environment is the condition $G > 2\gamma$, for which the crack velocity, v, is given by:

$$v = \frac{dc}{dt} = v_A \exp[(G - 2\gamma)/\eta] \quad (5)$$

where v_A is a velocity that increases with increasing chemical reaction rate at the crack tip and η is the thermal energy/bond area. Integration of Equation (5) leads to the time-dependent decrease between the maximum strength (Equation (2)) and the minimum strength (Equation (4)). Prior observation[5] and here shows that ψ and χ in Equations (1), (2), and (4) are not altered by exposure to H_2O, leading to straightforward numerical integration of Equation (5) in accord with Observation (2) above (an example is shown in Figure 1). The surprising point, Observation (4), is that, prior to the incubation time, the atomic-scale bond rupture kinetic parameters (v_A, 2γ, η) in Equation (5) appear to be unaffected by the BHF solution relative to H_2O: the reactive strengths are identical. It is beyond the scope of this work, but the similarity of the inert and reactive strength increases after the incubation time suggests that the insertion of Equations (3a) and (3b) into Equation (1) and hence Equation (5) would lead to the correct reactive strength variation with exposure time (after numerical integration; simple multiplication enabled the solid line in Figure 4). The important point to note here is that the corrosive environment affects strengths through the "mechanics" of the crack driving force not the "mechanisms" of the bond-rupture kinetics.

Finally, this last point has broad implications for approaches to brittle material reliability predictions. Traditionally, crack velocity measurements using long-crack specimens have been used to assess and predict brittle material reliability. The long cracks enable G to be well specified (e.g., cantilever beam specimens[13]) and v to precisely measured, thus establishing the $v(G)$ response and the parameters in Equation (5) in terms of environmental variables. The overwhelming majority of published work on glass and ceramic mechanical reliability is based on propagation of long, sharp cracks enhanced by weak corrosion; since the earliest observations the effect has been used in explanations of delayed failure.[19] Brittle material reliability predictions, however, require the integration of Equation (5) for very short cracks that control strength (e.g., contact flaws as in Figures 5, 7, 9, 11) for which $G(c)$ is required, and, in reality, often not simple. Assumptions of an incorrect $G(c)$ function will render a reliability prediction useless, no matter how well $v(G)$ is known. (A similar observation was made recently regarding the difficulty of implementing long-crack toughness measurements for short crack strength predictions.[32]) The observation here is that the additional time dependence included into $G(c)$ for strength- or reliability-controlling flaws in a moderately corrosive environment has a significant effect, even leading to strength or lifetime increases.

ACKNOWLEDGMENTS

The author thanks Eric Liniger for experimental assistance and Drs Lawrence Friedman and Frank DelRio for discussion of the manuscript. Certain commercial equipment, instruments, or materials are identified in this paper in order to specify the experimental procedure adequately. Such identification is not intended to imply recommendation or endorsement by the National Institute of Standards and Technology, nor is it intended to imply that the materials or equipment identified are necessarily the best available for the purpose.

ORCID

Robert F. Cook http://orcid.org/0000-0003-0422-8881

REFERENCES

1. Medvedovski E. Influence of corrosion and mechanical loads on advanced ceramic components. *Ceram Int*. 2013;39:2723-2741.
2. Luo H, Tang X, Dong Z, Tang Y, Nakamura T, Yatani H. The influence of accelerated aging on mechanical properties of veneering ceramics used for zirconia restorations. *Dent Mater J*. 2016;35:187-193.
3. Mould RE. Strength and static fatigue of abraded glass under controlled ambient conditions: III, Aging of fresh abrasions. *J Am Ceram Soc*. 1960;43:160-167.
4. Mould RE. Strength and static fatigue of abraded glass under controlled ambient conditions: IV, effect of surrounding medium. *J Am Ceram Soc*. 1961;44:481-491.
5. Cook RF. Multi-scale effects in the strength of ceramics. *J Am Ceram Soc*. 2015;98:2933-2947.
6. Lawn BR, Jakus K, Gonzalez AC. Sharp vs blunt crack hypothesis in the strength of glass: a critical study using indentation flaws. *J Am Ceram Soc*. 1985;68:25-34.
7. Cook RF. Strength and sharp contact fracture of silicon. *J Mater Sci*. 2006;41:841-872.
8. Cook RF, Roach DH. The effect of lateral crack growth on the strength of contact flaws in brittle materials. *J Mater Res*. 1986;1:589-600.
9. Roach DH, Cooper AR. Effect of contact residual stress relaxation on fracture strength of indented soda-lime glass. *J Am Ceram Soc*. 1985;68:632-636.
10. Han WT, Hrma P, Cooper AR. Residual stress decay of indentation cracks. *Phys Chem Glasses*. 1989;30:30-33.
11. Hrma P, Han WT, Cooper AR. Thermal healing of cracks in glass. *J Non-Cryst Solids*. 1988;102:88-94.

12. Han WT, Tomozawa M. Effect of residual water in silica glass on static fatigue. *J Non-Cryst Solids*. 1991;127:97-104.
13. Wiederhorn SM, Bolz LH. Stress corrosion and static fatigue of glass. *J Am Ceram Soc*. 1979;53:543-548.
14. Saha CK, Cooper AR Jr. Effect of etched depth on glass strength. *J Am Ceram Soc* 1984;67:C-158-C-159.
15. Danyluk S, Lee S-W. Surface states and the temperature dependence of microindentation damage in silicon. *J Appl Phys*. 1988;64:4075-4081.
16. Thouless MD, Cook RF. Stress-corrosion cracking in silicon. *Appl Phys Lett*. 1990;56:1962-1964.
17. Almond EA, May AT, Roebuck B. Stress corrosion cracking of a 6% cobalt/tungsten carbide hard metal. *J Mater Sci*. 1976;11:565-568.
18. Roach DH, Cooper AR. Weakening of soda-lime glass by particle impact during hydrofluoric acid etching. *J Am Ceram Soc* 1986;69:C-153-C-155.
19. Charles RJ, Hillig WB. The kinetics of glass failure by stress corrosion. In *Symposium on Mechanical Strength of Glass and Ways of Improving It*. Charleroi, Belgium: Union Scientifique Continentale du Verre, 1962;511-527.
20. Chuang T-J, Fuller ER Jr. Extended Charles-Hillig theory for stress-corrosion cracking of glass. *J Am Ceram Soc*. 1992;75:540-545.
21. Hillig WB. Model of effect of environmental attack on the flaw growth kinetics of glass. *Int J Fract*. 2007;143:219-230.
22. Orowan E. The fatigue of glass under stress. *Nature*. 1944;154:341-343.
23. Lawn BR. An atomistic model of kinetic crack growth in brittle solids. *J Mater Sci*. 1975;10:469-480.
24. Cook RF, Liniger EG. Kinetics of indentation cracking in glass. *J Am Ceram Soc*. 1993;76:1096-1106.
25. Cook RF. Toughening of a cordierite glass-ceramic by compressive surface layers. *J Am Ceram Soc*. 2005;88:2798-2808.
26. Roark RJ, Young WC. *Formulas for Stress and Strain*, 5th edn. Tokyo: Japan. McGraw-Hill; 1983.
27. Cook RF. Fracture mechanics of the scratch strength of polycrystalline alumina. *J Am Ceram Soc*. 2017;100:1146-1160.
28. Chantikul P, Anstis GR, Lawn BR, Marshall DB. A critical evaluation of indentation techniques for measuring fracture toughness: II. Strength method. *J Am Ceram Soc*. 1981;64:539-543.
29. Cook RF, Pharr GM. Direct observation and analysis of indentation cracking in glasses and ceramics. *J Am Ceram Soc*. 1990;73:787-817.
30. Matthewson MJ, Kurkjian CR. Environmental effects on the static fatigue of silica optical fiber. *J Am Ceram Soc*. 1988;71:177-183.
31. Kurkjian CR, Matthewson MJ, Rooney JM. Effects of heat treatment and HF etching on the strength of silica waveguides. In *Reliability of Optical Fiber Components, Devices, and Networks II*. SPIE, Bellingham, WA, 2004;223-229.
32. Marshall DB, Cook RF, Padture N, et al. The case for indentation as an enduring and exploratory characterization tool. *J Am Ceram Soc*. 2015;98:2671-2680.

How to cite this article: Cook RF. Strength of brittle materials in moderately corrosive environments. *J Am Ceram Soc*. 2018;101:1684–1695. https://doi.org/10.1111/jace.15307